



Experimental study of a counter-flow jet in onera's S1MA wind tunnel by 3D background oriented Schlieren

Francois Nicolas, David Donjat, Francis Micheli, Guy Le Besnerais, Aurelien Plyer, Philippe Cornic, Frédéric Champagnat, Yannick Michou

► To cite this version:

Francois Nicolas, David Donjat, Francis Micheli, Guy Le Besnerais, Aurelien Plyer, et al.. Experimental study of a counter-flow jet in onera's S1MA wind tunnel by 3D background oriented Schlieren. ISFV 18, Jun 2018, ZURICH, Switzerland. hal-02000679

HAL Id: hal-02000679

<https://hal.science/hal-02000679>

Submitted on 6 Feb 2019

HAL is a multi-disciplinary open access archive for the deposit and dissemination of scientific research documents, whether they are published or not. The documents may come from teaching and research institutions in France or abroad, or from public or private research centers.

L'archive ouverte pluridisciplinaire **HAL**, est destinée au dépôt et à la diffusion de documents scientifiques de niveau recherche, publiés ou non, émanant des établissements d'enseignement et de recherche français ou étrangers, des laboratoires publics ou privés.



EXPERIMENTAL STUDY OF A COUNTER-FLOW JET IN ONERA'S S1MA WIND TUNNEL BY 3D BACKGROUND ORIENTED SCHLIEREN

F. Nicolas¹, D. Donjat^{2,c}, Francis Micheli², Guy Le Besnerais³, Aurélien Plyer³, Philippe Cornic³,
Frédéric Champagnat³, Yannick Michou¹

¹ONERA, DS, BP25, 73500 Modane, France

²ONERA, DMPE, 2 Avenue Edouard Belin, 31400 Toulouse, France

³ONERA, DTIS, Chemin de la Hunière, 91123 Palaiseau, France

^cCorresponding author: Tel.: +33562252808; Fax: +33562252553; Email: david.donjat@onera.fr

KEYWORDS:

Main subjects: density measurement, flow visualization

Fluid: high speed flows

Visualization method(s): Background Oriented Schlieren

Other keywords: wind tunnel, counter flow jet

ABSTRACT: *This paper describes an application of 3D density reconstruction from a limited number of Background Oriented Schlieren (BOS) images in a large high speed wind tunnel. The tested flow is a counter-flowing hot jet facing the transonic main flow. Ray deviation maps captured by 12 synchronized cameras are combined to reconstruct the three dimensional density field of the jet, in the line of the direct 3D BOS technique proposed by ONERA.*

1 Introduction

Schlieren-based density field visualization techniques have been widely used in wind tunnels in order to understand fluid mechanics phenomena such as compressible or thermally-driven flows. Traditionally, Schlieren measurements have provided mainly qualitative information, but they have had somewhat limited use as validation data for fluid flow models or computational fluid dynamics codes. BOS is an emerging technique for quantitative measurement of density gradients, which even allows 3D density field reconstruction. Here we describe the first application of a multi-camera BOS technique for instantaneous 3D density field estimation in a trans-sonic wind tunnel facility in order to confirm the potential of 3DBOS for complex flow characterization in wind tunnel environment. The system is deployed in the large industrial wind tunnel S1MA located in ONERA's center of Modane (France).

1.1 3DBOS technique

The BOS technique relies on the measurement of the deviation of light rays propagating within an inhomogeneous index media as described in [4] and [5]. The BOS optical system is remarkably simple, consisting of a camera and a textured background located on either side of the studied flow. The procedure consists in recording a couple of images of the background, firstly without any flow (i.e. reference frame) and then with the flow in between the camera and the background. Ray deviation is derived from apparent displacement of the background patterns computed using cross-correlation

algorithms (as described in Figure 1). The measured deviation is proportional (with G , the Gladstone-Dale constant) to the integral of the density gradient along ray paths as given by Eq. 1.

$$\varepsilon = \frac{G}{n_{ext}} \int_{s \in ray} \nabla \rho ds \quad (1)$$

Indeed, unlike Schlieren or Digital Holography, BOS technique does not require a sophisticated optical apparatus ensuring a parallel light beam. Therefore, its field of view is not limited by the size of expensive optics (lens or parabolic mirrors) and large phenomena can be imaged. Finally, the BOS technique is particularly suited to experimental facilities such as wind tunnels where it offers a very interesting way to characterize complex flows.

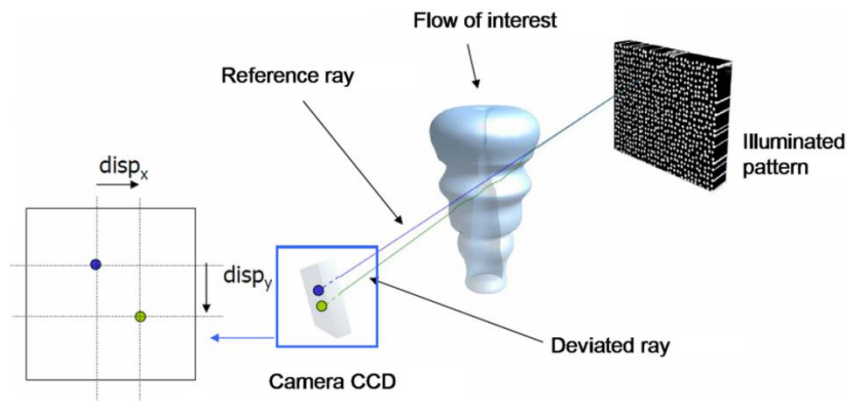


Fig. 1. Sketch of the BOS setup

The extension to 3D reconstruction requires the acquisition of several deviation maps recorded with various viewpoints and a numerical inversion of the Eq. 1 as proposed by [6] and [7]. In [1], we described a 3D reconstruction of the density based on simultaneous acquisitions of the flow by several cameras. Good results were obtained with 12 cameras on aerothermal test cases showing weak density gradients, conditions which ensure the validity of the paraxial hypothesis for ray trajectories [2]. Finally, in [3], 3D reconstruction of an under expanded jet in lab environment shed some light on the validity of the direct 3DBOS method in the context of compressible flows.

1.2 Application of BOS and 3DBOS in wind tunnels

Few years ago, NASA investigated BOS in their ground test facilities. In a first experiment realized by Schairer et al [8] used Retro-Reflective Background-Oriented Schlieren (RBOS) to detect a rotor wing tip vortex in the National Full-Scale Aerodynamics Complex at NASA Ames Research Center. Then several tests were conducted in different facilities at NASA Langley Research Center [9], where the focus was put on evaluating and optimizing the sensitivity of the technique. Finally, in [10] BOS provided density profiles in the separated flow around a re-entry capsule in a subsonic wind tunnel. The DLR has also applied the BOS technique in different facilities. In [11], BOS measurements are performed in the high enthalpy shock tube in Göttingen and 2D measured displacements are shown to be in good agreement with CFD simulation results. In [12], 2D BOS is applied within an industrial wind tunnel to investigate the density gradients in the slipstream of a nine bladed propeller model. In

[13], the DLR proposed a large scale and time-resolved visualization of a scale 1:1 engine jet flow with a 2D BOS system composed of four synchronized high-speed cameras and pulsed LED illumination. Nevertheless, all previously reviewed approaches are restricted to 2D BOS. In first adaptations of 3DBOS technique in a wind tunnel environment, the authors conduct repeated acquisitions by a unique camera which is rotated around the jet, a process which is restricted to stationary or periodic flows. For example, Leopold et al. [7] reconstructed a supersonic flow around a spike at ISL with the color BOS technique. Closer to our context, Hartmann and Seume [14] used an 8-camera BOS setup to detect density anomalies in a jet for helicopter engine maintenance application. Using a combination of FBP and ART reconstruction techniques, they are able to reduce tomographic artifacts related to the limited number of views and to relate local density gradients to some defect of the compressor. As a result, their experimental study is focused on detection rather than on quantitative temperature or density field estimation. Here, we propose to adapt a similar measurement set up presented in [2] in the large transonic wind tunnel S1MA in order to shed light on the capability of this new technique to describe large and complex wind tunnel flows.

2 Experimental setup

2.1 S1 wind tunnel: a giant

The S1MA wind tunnel located at ONERA in Modane (French Alps) is the largest continuous-flow and atmospheric transonic wind tunnel with a return circuit in Europe. The test section is 14 m long and has a circular cross section with a diameter of 8 m. The Mach number is continuously adjustable from 0.05 to 1 with a $P_i=0.9$ bar and maximum $T_i=333$ K. The wind tunnel, shown in figure 2 and schematically represented in figure 3, is composed of three interchangeable test sections. One of them is dedicated to the optical measurement systems as PSP and MDM. It is equipped with several windows distributed around the test section, which provide a reasonable access for optical diagnostics.



Fig. 2. S1MA wind tunnel at ONERA center in Modane

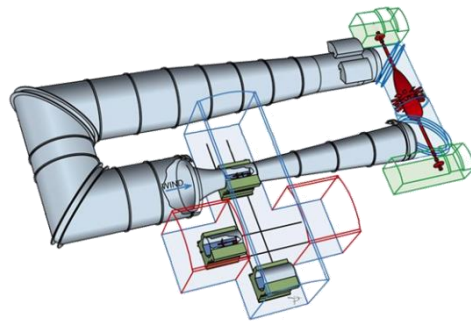


Fig. 3. Sketch of S1MA wind tunnel with the three test sections and fans

For this experiment, the model under study is an air ejector (with a diameter of 80 mm) fixed to a tripod sting holder and facing the main transonic flow, as shown in figure 4. This unusually configuration is a model of supersonic retro propulsion configuration involved in the reentry path flight control of space vehicles.

The pipe is fed with high pressure air (HP), warmed up by a heater to 340K. Due to the complexity of HP distribution circuit, a perforated conical sheet, localized close to the exit, is used to optimize the homogeneity of the air exiting from the nozzle. Pressure and static temperature are followed in the outlet of it. A whole set of conditions has been investigated by varying the wind tunnel Mach number (between 0 to 0.85) and the nozzle mass flow rate Q (between 0 to 3 kg.s^{-1}). In a second part of the campaign, a configuration with a double nozzle, composed of two pipes with a diameter of 56.6 mm each, was also tested.

2.2 3DBOS set-up

For 3DBOS acquisitions in S1MA, 12 cameras JAI BM-500GE (5 Mpixel sensor with $3.45 \text{ }\mu\text{m}$ pixels) equipped with a 70 mm focal length Schneider C-mount optics were used. Cameras are all synchronized with the illumination generators which are fed by a Nd:YAG laser source (allowing short time effective exposure (100 ns) in order to freeze the flow) coupled with an ad hoc division plate which separates the laser beam into 8 and directs them into liquid light guides (see [2] for further details). Liquid guides reduce speckle noise that could degrade images information content while still transmitting 80 % of the incident light. All optical devices are distributed on a nearly half-ring shape, a standard configuration for jet flows studies [2], around the test section behind several windows as shown in figure 4.

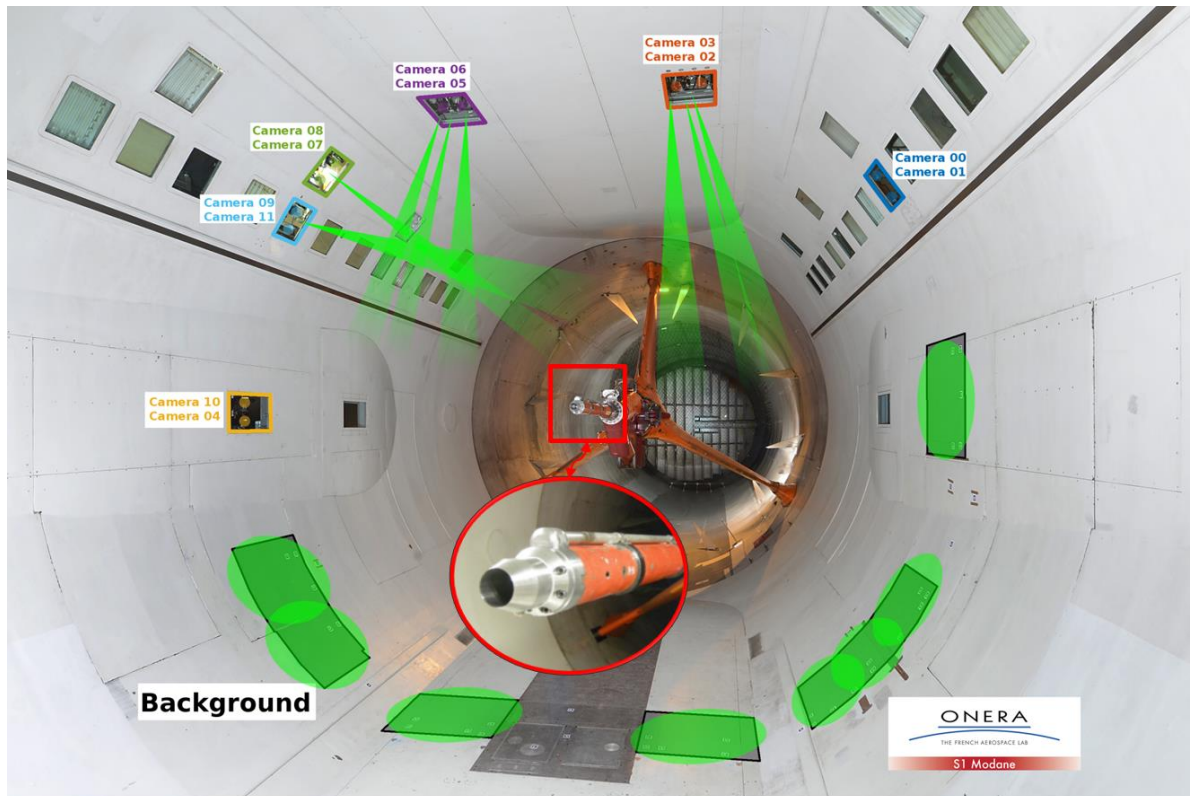


Fig. 4. Sketch of the BOS setup

Cameras are positioned per pair behind each window and linked to a computer via an Enterasys switch and synchronized with a TTL generator which can handle 24 independent signals. During the acquisition, images are transferred to RAM memory and then stored onto fast SSD disks. This solution enables us to acquire 900 images at 10 Hz for each tested conditions. The background panels, covered with a semi-random distribution of 1 mm diameter white dots, are located on the test section's floor on a surface of about 10 m².

2.3 Difficulties and drawbacks

In this kind of environment, the setting up of optical diagnostic as 3D BOS is a serious challenge. Several drawbacks can be listed:

- Optical windows are small and their numbers reduced
- Background panels, glued on the test section's floor, have to endure a Mach 0.85 flow.
- The illumination of a very large background surface have to be ensured
- Due to friction on wind tunnel walls and despite air exchange with atmosphere for cooling, the temperature of the main flow can reach 50°C. This temperature increase induced wall dilatation and background panels weakness
- For high Mach number, fans induce very large wall vibrations.

In order to prevent the influence of perturbations generated by the wind tunnel, vibration amplitudes are initially measured with an accelerometer localized on a single camera. As shown on figure 5, camera vibration is defined by a low frequency behavior around 55 Hz. According to this first analysis, each optical system is set on suitable anti-vibration mounts.

Moreover, in order to evaluate the wall displacements, several AprilTags markers are glued on each coin of backgrounds (as illustrated on figure 6) in order to be tracked during image acquisition. In this way, an estimation of their displacement could be used as an image correction. In addition, these markers could also be used with a stereo photogrammetry set up in order to obtain a 3D reconstruction of the test section's geometry which provides an evaluation of the wall dilatation; an example of reconstruction of the test section for atmospheric conditions is presented in figure 6.

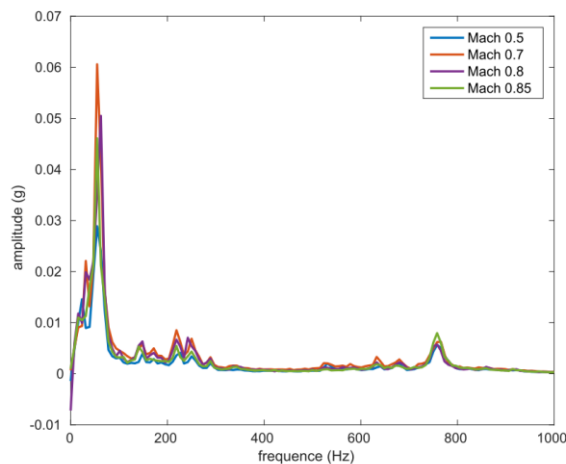


Fig. 5. Structural vibration analysis according to flow Mach number in S1MA

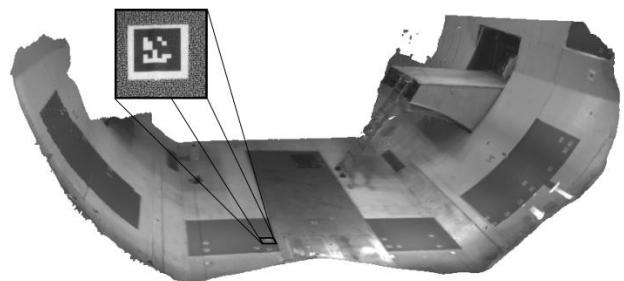


Fig. 6. 3D reconstruction of the test section based on stereo photogrammetry

Despite the use of a Nd:YAG laser as illumination source, the size of backgrounds and the lack of light imposed to enlarge the cameras aperture which is finally fixed to $f\#=2$. This choice reduces the depth of field. In consequence, as each camera is focused on the background panel facing it, the measured volume (corresponding to a 50 cm cube) is outside the depth of field and then subject to a "geometric blur" which can be modeled as a circle of confusion of diameter 18 mm (see [17] and [3] for further details).

3 DBOS reconstruction process

3.1 Calibration

Tomographic reconstruction requires an accurate geometrical calibration of the multi-camera system in order to ensure geometric consistency of the different views. This process consists in identifying all cameras internal parameters (focal lengths, principal points, distortion parameters) and all cameras poses (position and orientation) in the same coordinate frame. Calibration developments specific to the 3DBOS have been discussed in [19]. With a half-ring configuration, it is difficult to ensure that the calibration body is visible for all cameras at once. Hence the 2D calibration plate is moved inside the measured volume and the calibration process exploits a chain of dependencies between views having a sufficient number of calibration features in common. This way, a global geometric calibration with respect to a unique reference coordinate frame can be found. For SIMA tests, a large calibration plate was specifically designed for the experiment as illustrated by the figure 7. The first image is important since it defines the reference coordinate system which is fixed to the measurement volume. Its origin is located here in the center of the nozzle outlet. The calibration process used the exploitable images recorded by all cameras for 70 different locations of the calibration target. At the end of the optimization, the mean reprojection error is 0.42 pixels with a standard deviation of 0.34 pixels (see figure 7).

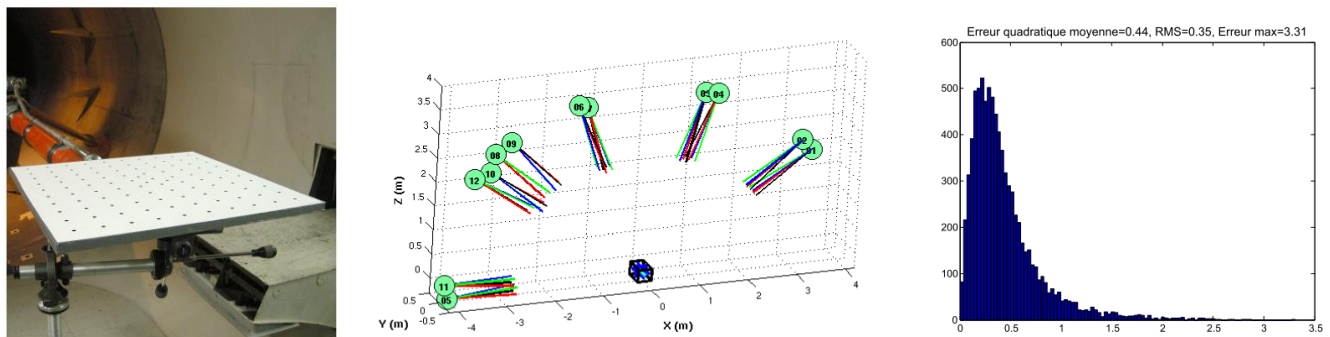


Fig. 7. Calibration process – Left : calibration plate in the referential position – In the middle : positioning of all BOS cameras around the measured volume given by calibration process – Right : quality of global calibration

3.2 Tomography

By using the calibration model previously obtained, distortion-corrected images are generated, which satisfy a pinhole camera model with straight projection rays. Displacements are measured between patterns of images acquired across the flow and patterns of reference images acquired without the flow by numerical cross-correlation methods (with the ONERA's software called

FOLKI-SPIV [18]). Deviation maps are then computed from estimated displacements using the approximation that the deviation occurred at the mid-point of the investigated volume. Finally, they are combined into the 3D reconstruction of the density volume using the direct tomographic method proposed in [1] and quickly described here.

Assuming that the paraxial approximation applies, the integral relation between deviation and density defined by Eq. 1 can be cast as a linear system (defined by Eq. 2) where the observation operator A combines the spatial derivative D of the density volume ρ and the tomographic operator T associated to the imaging process.

$$\varepsilon = A\rho \quad (2)$$

As the observation operator A is non regular and ill-conditioned, regularization tools are required to define a unique and well-behaved solution. The density estimate is then defined as the minimizer of a compound criterion formed with the classical least-squares term and a smoothing Tikhonov-type term [20]:

$$J(\rho) = \|\varepsilon - A\rho\|^2 + \lambda\|\nabla\rho\|^2 \quad (3)$$

The balance between data and regularization terms is controlled by the regularization parameter λ , which could be tuned using the L-curve technique (more details can be found in [21]). For both inlet and outlet boundaries, free boundary conditions are imposed to ensure the consistency of the reconstruction.

Minimization of J in Eq. 3 uses a conjugate gradient method. Note that we use a user-defined 3D mask to limit the number of voxels which are updated in the optimization process, a key point to improve the efficiency of the calculation. Finally, the algorithm is encoded on GPU architecture to reduce the computing time and to allow reconstruction of large fields.

3.2 Corrections

Whereas vibration influences are prevented with the help of anti-vibration mounts, unexpected additional wall effects, linked to the test section movements under aerodynamic efforts, interfered with density gradient-based displacement measured by BOS. Indeed, the figure 8 shows the evolution of a mean global displacement detected on each displacement map generated by BOS, with the increase of the wind tunnel Mach number.

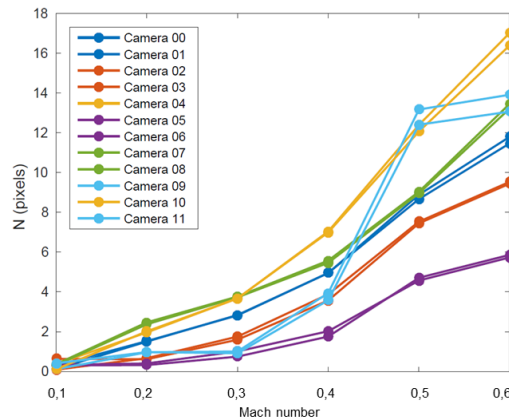


Fig. 8. Evolution of the mean global displacement observed by BOS with the increase of main flow Mach number

Due to the very hard experimental conditions for optical measurements exposed in 2.3, image acquisitions and post-treatment method had to be upgraded in order to reduce the influence of the aerodynamics efforts which generate the deformation of the test section's walls. In this way, by considering the equivalent translation for a same Mach number configuration, the BOS displacement maps obtained with a working jet were corrected by subtracting the mean global displacement induced by the wind tunnel flow and measured without the jet.

4 Experimental results and discussion

Tests are conducted for several freestream Mach numbers comprised between 0 and 0.85, and nozzle flow rates comprised between 0 and 3 kg/s. The 3D reconstructions of density field are obtained according to the mean deviation maps calculated with 900 images (with an acquisition rate of 10 Hz).

4.1 Without wind tunnel flow

Figure 9 shows the maps of instantaneous and averaged displacements of the pattern for several nozzle mass flow rates. The plume ejected by the nozzle comes from the left of the map. As the mass flow rate of the nozzle increases, the complex jet topology appears clearly with shock cells and acoustic waves generated at the nozzle's lips.

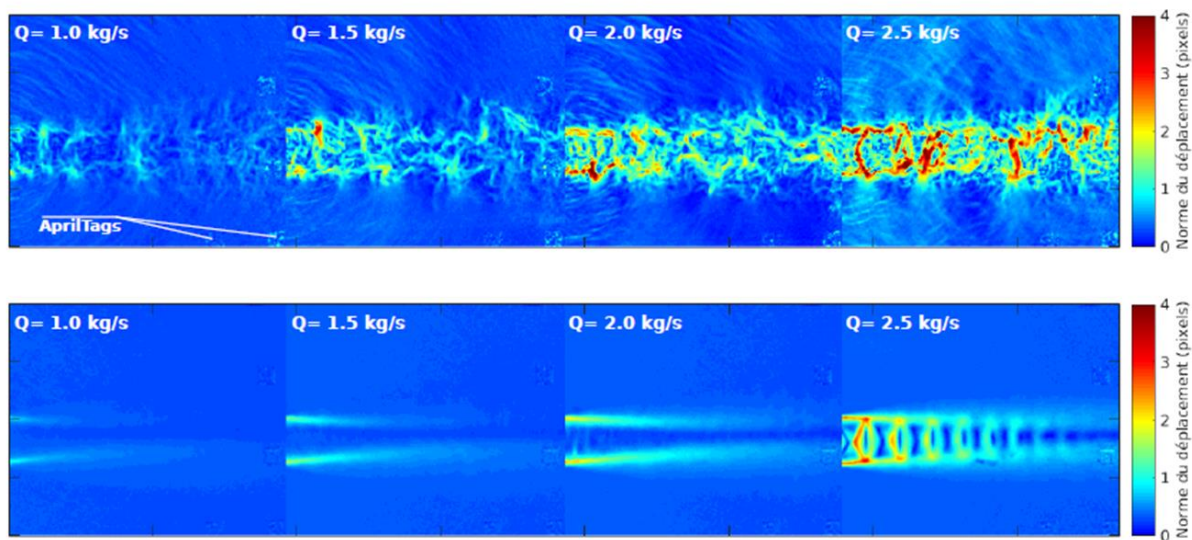


Fig. 9. Map of the instantaneous displacement norm (top) and averaged displacement norm (bottom) for several nozzle mass flow rates (between 1 and 2.5 kg/s)

The compressible topology of the plume is also clearly visible on averaged maps, particularly for highest mass flow rates. In particular, for 2.5 kg/s, the mean field is similar to a moderately under-expanded jet as the train of shock waves is detected in the potential core region. This pattern results from the successive reflection of expansion fans and shock waves on the jet boundary. Compared to the instantaneous map, the two first shock-cells on the left which seems to stabilize the beginning of the plume are well observed.

A 3D reconstruction of the free jet is performed for this last configuration and presented on figure 10. The calculation is performed on a volume equals to 450 mm x 250 mm x 250 mm discretized with 30 M voxels.

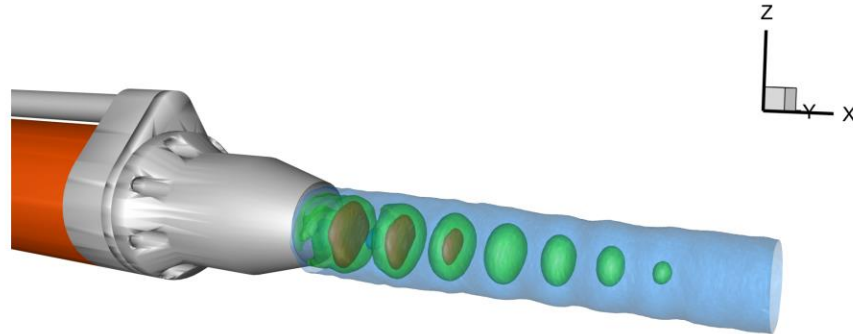


Fig. 20. Density field of the 2.5 kg/s jet and Mach number 0

The result is consistent with the under expanded topology and comparable with jet flows measured in [3].

4.2 With wind tunnel flow

The figure 11 gives an example of the behavior of the jet when the double nozzle plume is impinged by the main transonic air flow. In this configuration where the main flow reaches Mach 0.85, the jet is stopped in the vicinity of the outlet and an intense unsteady shock wave appears in front of it. Such visualizations open the way to finer analysis of unsteady behavior of complex compressible interaction.

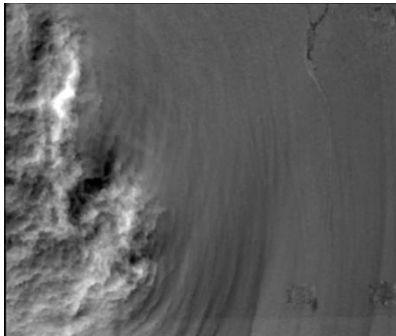


Fig. 31. Map of displacements for $Q=3$ kg/s and $M=0.85$

The Figure 12 shows the 3D reconstruction of the jet, with a mass flow rate of 1 kg/s, impinged by the main flow (with $M=0.4$). As in 2D visualization, this view shows that the jet is quickly stopped by the main flow and reversed, giving a specific mushroom shape to density's isosurfaces. Moreover, the range of density measured with 3DBOS is consistent with the estimation defined during the design of the experiment.

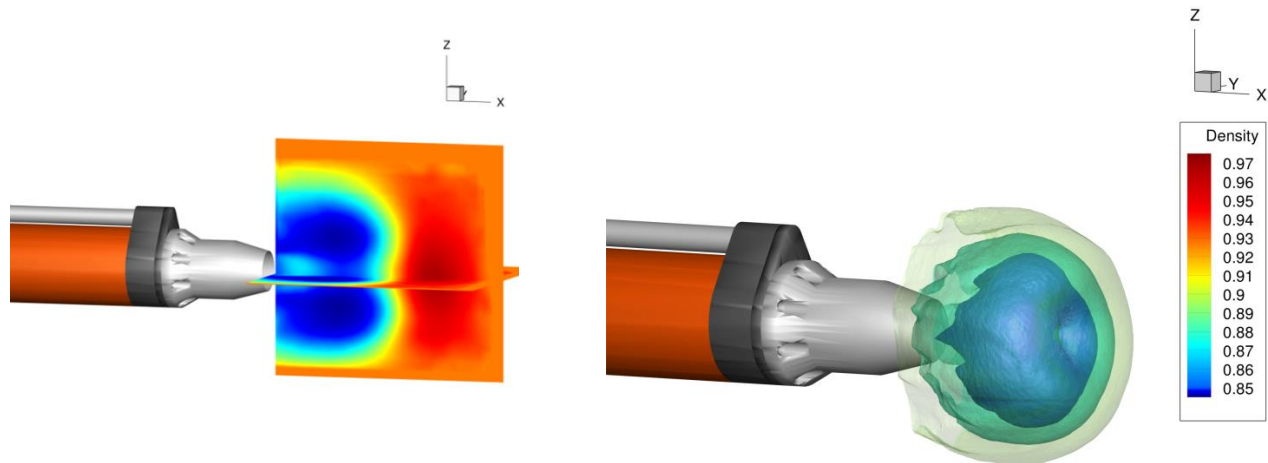


Fig. 42. 3D reconstruction of the jet ($Q=1\text{kg/s}$) impinging the main wind tunnel's flow ($M=0.4$) – Isosurfaces of density.

5 Conclusion

For the first time and despite inherent major difficulties, a BOS experiment involving 12 cameras mounted around a counter-flowing jet has been conducted in a very large wind tunnel environment. From the collections of corrected BOS deviation fields, 3D reconstructions of mean density fields have been obtained using the 3DBOS method of [1]. The mean density field obtained is consistent with the expected physical topology. Further evolutions of this technique for wind tunnel applications focus on the improvement of the illumination and image correction to balance backgrounds deformations and vibration effects.

Finally, this work is highlighted the potential of 3DBOS to provide the full 3D density field in compressible flows for such experimental installations. Further improvements will concern the ability of the technique to keep sufficient accuracy with a lower number of points of view. The ability of the technique to take into account a model is another challenge for this technique.

References

- [1] Nicolas F., Todoroff V., Plyer A., Le Besnerais G., Donjat D., Micheli F., Champagnat F., Cornic P., and Le Sant Y. *A direct approach for instantaneous 3D density field reconstruction from background-oriented schlieren (BOS) measurements*. Experiments in Fluids, 57(1):1–21, 2016.
- [2] Nicolas F., Donjat D., Plyer A., Champagnat F., Le Besnerais G., Micheli F., Cornic P., Le Sant Y., and Deluc J.-M. *Experimental study of a co-flowing jet in ONERA's F2 research wind tunnel by 3D Background Oriented Schlieren*, MST 28(8), 2017
- [3] Nicolas F., Donjat D., Leon O., Le Besnerais G., Champagnat F., and Micheli F. *3D reconstruction of a compressible flow by synchronized multi-camera BOS*. Experiments in Fluids, 58(46), 2017.
- [4] Meier G. *Computerized background-oriented Schlieren*. Experiments in Fluids, 33(1):181–187, 2002.
- [5] Raffel M. *Background-oriented schlieren (BOS) techniques*. Experiments in Fluids, 56(3):1–17, 2015.
- [6] Atcheson B., Ihrke I., Heidrich W., Tevs A., Bradley D., Magnor M., and Seidel H.-P. *Time-resolved 3D capture of non-stationary gas flows*. ACM Trans. Graph., 27(5):132:1–132:9, December 2008.
- [7] Leopold F., Ota M., Klatt D., and Maeno K. *Reconstruction of the unsteady supersonic flow around a spike using the colored background oriented schlieren technique*. Journal of Flow Control, Measurement & Visualization, 1(2):69–76, 2013.

- [8] Schairer E., Kushner L.K., and Heineck J. T.. *Measurements of tip vortices from a full-scale uh-60a rotor by retro-reflective background oriented schlieren and stereo photogrammetry*. In 69th American Helicopter Society Annual Forum, Phoenix (USA), 2013.
- [9] Bathel B.F., Borg S., Overmeyer A., Walker E., Gad W., Clem M., Schairer E.T. and Mizukaki T. *Development of background oriented schlieren for NASA Langley research center ground test facilities*. In 53rd AIAA SciTech, Kissimmee (USA), 2015.
- [10] Mizukaki T., Borg S., Danehy P.M., Murman S.M., Matsumura T., Wakabayashi K. and Nakayama Y.. *Background-oriented schlieren for large-scale and high speed aerodynamic phenomena*. In AIAA SciTech, Kissimmee (USA), 2015.
- [11] Kirmse T., Agocs J., Schröder A., Martinez Schramm J., Karl S., and Hannemann K.. *Application of particle image velocimetry and the background-oriented Schlieren technique in the high-enthalpy shock tunnel Göttingen*. Shock Waves, 21:233–241, 2011.
- [12] Roosenboom E.W.M., Geisler R., Agocs J., Schanz D., Weikert T., Kirmse T., and Schröder A.. *Assessment of propeller induced properties and active flow control using multiple image-based measurement systems*. In PIV13, Delft (The Netherlands), 2013.
- [13] Geisler R., Schröder A., Schanz D., Agocs J., and Siller H. *Large scale density gradient visualization of the v2527 engine jet flow at ground operation using background oriented schlieren (BOS)*. In AIAA SciTech, San Diego (USA), 2016.
- [14] Bauknecht A., Ewers B., Wolf C., Leopold F., Yin J., and Raffel M.. *Three-dimensional reconstruction of helicopter blade tip vortices using a multi-camera BOS system*. Exp. Fluids, 56(1):1–13, 2015.
- [15] Hartmann U. and Seume J.R., *Combining ART and FTP for improved fidelity of tomographic BOS*, MST 27(9), 2016
- [16] Goldhahn E. and Seume J.. *The background oriented Schlieren technique: sensitivity, accuracy, resolution and application to a three-dimensional density field*. Experiments in fluids, 43:241–249, 1998.
- [17] Gojani A. B., Kamishi B., and Obayashi S.. *Measurement sensitivity and resolution for background oriented schlieren during image recording*. Journal of Visualization, 16(3):201–207, 2013.
- [18] Champagnat F., Plyer A., Le Besnerais G., Davoust S., and Le Sant Y. *Fast and accurate PIV computation using highly parallel iterative correlation maximization*. Experiment in Fluids, 50:1169–1182, 2011.
- [19] Le Sant Y., Todoroff V., Bernard-Brunel A., Le Besnerais G., Micheli F., and Donjat D. *Multi-camera calibration for 3DBOS*. In Application of Laser Techniques to Fluid Mechanics, Lisbon (Portugal), 2014.
- [20] Tikhonov A. and Arsenin V. *Solutions of ill-posed problems*. Winston, 1977.
- [21] Hansen P. C. *Analysis of discrete ill-posed problems by means of the l-curve*. SIAM review, 34(4):561–580, 1992.

Copyright Statement

The authors confirm that they, and/or their company or institution, hold copyright on all the original material included in their paper. They also confirm they have obtained permission, from the copyright holder of any third-party material included in their paper, to publish it as part of their paper. The authors grant full permission for the publication and distribution of their paper as part of the ISFV18 proceedings or as individual off-prints from the proceedings.